Hu, H., Li, J.W., Harlov, D., Lentz, D., McFarlane, C. and Yang, Y.H., 2019. A genetic link between iron oxide-apatite and iron skarn mineralization in the Jinniu volcanic basin, Daye district, eastern China: Evidence from magnetite geochemistry and multi-mineral U-Pb geochronology. GSA Bulletin, https://doi.org/10.1130/B35180.1.

Data Repository

Figure DR1. TIMA-X TESCAN integrated mineral analyzer images of iron skarn (A) and IOA ores (B).

Figure DR2. The paragenetic sequence of mineralization and alteration of the Wangbaoshan iron deposit.

Figure DR3. X-ray element distribution maps showing the texture of typical garnet in the iron skarn ore. The color scale bar in EMPA maps represents the intensity of collected X-ray counts.

Figure DR4. The plot of Na-Ca-Fe-K-Mg code bars on an alteration discrimination diagram from Montreuil et al. (2013). Chemical data from Mao et al. (2011) and references therein; Xie et al. (2012); Chen et al. (2014, 2016). Note: Most of the igneous rock in the Ningwu and Luzong district are plotted in the field of least alteration. This indicates that the high K contents of most igneous rocks related to IOA and iron skarn deposits reflect a metasomatized lithospheric mantle source for the magma rather than being caused by potassic alteration. Unlike the extensive albitization in the Wangbaoshan ore district, the volcanic rocks far away from the iron mine in this region are mostly fresh. The granitoid host rock surrounding the iron skarn often shows sodic alteration.

Figure DR5. Ternary diagrams of garnet and pyroxene end members from iron skarns and IOA ores. Gr—grossular, Pyr—pyralspite, Ad—andradite, Di—diopside, Hd—hedenbergite, Jo—johannsenite. The composition of garnets and pyroxenes from the Chengchao and Jinshandian iron deposits, and the Fe skarn deposits worldwide are adapted from Xie et al. (2015) and Meinert et al. (2005).

Table DR1. Electron microprobe analyses (wt%) of magnetite from iron skarn and iron oxide-apatite ores from the Wangbaoshan iron deposit, and the Meishan and Wangmujian prospects.

Table DR2. LA-ICP-MS trace element compositions of magnetite from iron skarn and iron oxide-apatite ores in the Wangbaoshan iron deposit.

Table DR3. Major and trace element compositions of iron skarn and iron oxide-apatite (IOA) ores from the Wangbaoshan iron deposit and typical IOA ores from the Meishan and Wangmujian prospects.

Table DR4. Electron microprobe analyses (wt%) of garnet and diopside from iron skarn and iron oxide-apatite ores from the Wangbaoshan iron deposit.

Table DR5. LA-ICP-MS zircon U-Pb dating of diorite porphyry from the Wangbaoshan iron deposit, Daye district.

Table DR6. LA-ICP-MS titanite U-Pb dating of IOA and iron skarn ores in the Wangbaoshan iron deposit, Daye district.

Table DR7. LA-ICP-MS fluorapatite U-Pb dating of IOA ores in the Meishan and Wangmujian prospects, Daye district.

APPENDIX 1

Methods

Thin sections mapping

Typical iron skarn thin section (WBS14) and IOA ore thin section (15WBS1) were analyzed using the Tescan Integrated Mineral Analyzer (TIMA) mineralogy system at the Tescan Orsay Holding demo lab, Czech Republic. The TIMA operating system comprises a Tescan Mira Schottky field emission scanning electron microscope with four silicon drift energy dispersive (EDS) detectors. TIMA analyses were conducted at operating conditions of 25 keV using a spot size ~50 nm, a working distance of 15 mm and a field size set at 1500 μm. The BSE image is obtained and used to determine individual particles and to determine boundaries between distinct preliminary phases. The EDX collected for each pixel is summed together based on grain boundaries. The spectroscopic data is then matched to mineral definition files within the TIMA classification scheme, where a set of rules must be satisfied for a phase to be correctly matched. This systematic identification of each grain allows for mineral phases within the sample to be identified and mapped. The mineral definition files contain mineral properties that can be used to determine the elemental composition, elemental deportment and density of the sample.

Electron microprobe analysis of garnet and diopside

A typical iron skarn sample (WBS14) and an IOA ore sample (WBS10) were collected for electron microprobe analysis (EMPA) and X-ray mapping of garnet and diopside in two sessions. Session 1 major-element analysis were determined using a CAMECA SX100 electron microprobe (EMP) analyzer (Masaryk University, Brno) at an accelerating voltage of 15 kV, a beam current of 20 nA, and a beam diameter of 3 μm. The following standards were used for garnet and diopside: albite (Na), sanidine (Al and K), wollastonite (Si and Ca), pyroxene (Mg), anatase (Ti), chromite (Cr), almandine (Fe), and spessartine (Mn). Session 2 was performed at the Center for Material Research and Analysis, Wuhan University of Technology (WUT), using a JXA-8230 Superprobe. Standards and unknowns were analyzed with 1 μm beam diameter at 15 kV and 20 nA current. The peak counting time for all the elements were 20 s. The following standards were used: $NaAlSi_3O_8$ (Na), $KAlSi_3O_8$ (K), $Mg_3Al_2Si_3O_{12}$ (Mg, Al and Si), (Ca, Fe)SiO_3 (Ca), $MnSiO_3$(Mn), $FeTiO_3$ (Fe, Ti) and $FeCr_2O_4$ (Cr).

REFERENCES CITED

Chen, L., Zhao, Z.F., and Zheng, Y.F., 2014, Origin of andesitic rocks: Geochemical constraints from Mesozoic volcanics in the Luzong basin, South China: Lithos, v. 190-191, p. 220–239, https://doi.org/10.1016/j.lithos.2013.12.011.

Chen, L., Zheng, Y.F., and Zhao, Z.F., 2016, Geochemical constraints on the origin of Late Mesozoic andesites from the Ningwu basin in the Middle-Lower Yangtze Valley, South China: Lithos, v. 254-255, p. 94–117, https://doi.org/10.1016/j.lithos.2016.03.012.

Mao, J.W., Xie, G.Q., Duan, C., Pirajno, F., Ishiyama, D., and Chen, Y.C., 2011, A tectono-genetic model for porphyry-skarn-stratabound Cu-Au-Mo-Fe and magnetite-apatite deposits along the Middle-Lower Yangtze River Valley, Eastern China: Ore Geology Reviews, v. 43, p. 294–314, https://doi.org/10.1016/j.oregeorev.2011.07.010.

Meinert, L.D., Dipple, G.M., and Nicolescu, S., 2005, World skarn deposits: Economic Geology 100th Anniversary Volume, p. 299–336, https://doi.org/10.5382/AV100.11.

Montreuil, J.-F., Corriveau, L., and Grunsky, E., 2013, Compositional data analysis of IOCG systems, Great Bear magmatic zone, Canada: To each alteration type its own geochemical signature: Geochemistry Exploration Environment Analysis, v. 13, p. 229–247, https://doi.org/10.1144/geochem2011-101.

Xie, G.Q., Mao, J.W., Zhao, H.J., Duan, C., and Yao, L., 2012, Zircon U-Pb and phlogopite 40Ar-39Ar age of the Chengchao and Jinshandian skarn Fe deposits, southeast Hubei Province, Middle-Lower Yangtze River Valley metallogenic belt, China: Mineralium Deposita, v. 47, p. 633–652, https://doi.org/10.1007/s00126-011-0367-2.

Xie, G.Q., Mao, J.W., Zhu, Q.Q., Yao, L., Li, Y.H., Li, W., and Zhao, H.J., 2015, Geochemical constraints on Cu-Fe and Fe skarn deposits in the Edong district, Middle-Lower Yangtze River metallogenic belt, China: Ore Geology Reviews, v. 64, p. 425–444, https://doi.org/10.1016/j.oregeorev.2014.08.005.

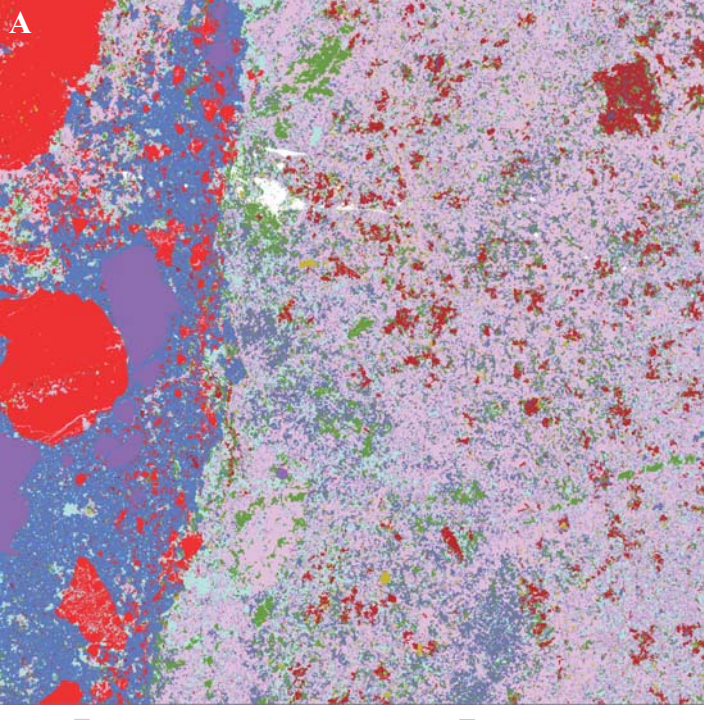
A
Calcite
Quartz-calcite fine grained mixture
Magnetite
Quartz
Garnet
Pyroxene
Chlorite
Titanite
Pyrite
Apatite

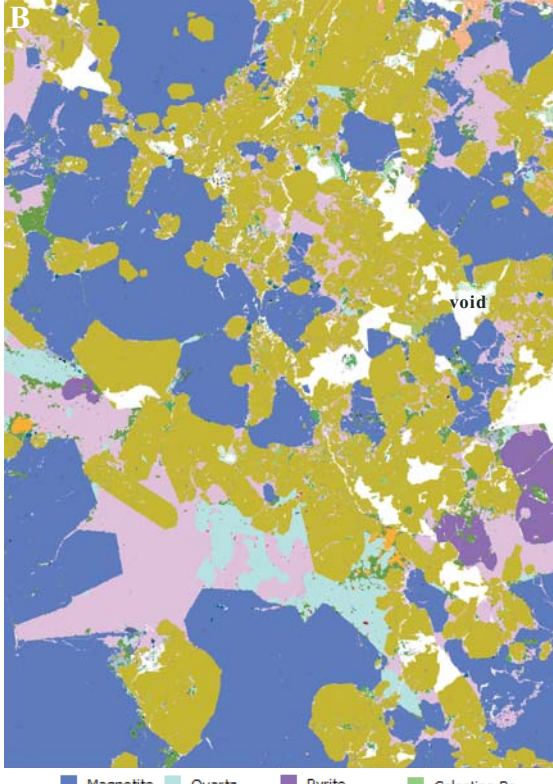
B
void
Magnetite
Apatite
Calcite
Quartz
Chlorite
Dolomite
Pyrite
Anhydrite
Biotite
Celestine-Ba
Rutile
Ilmenite

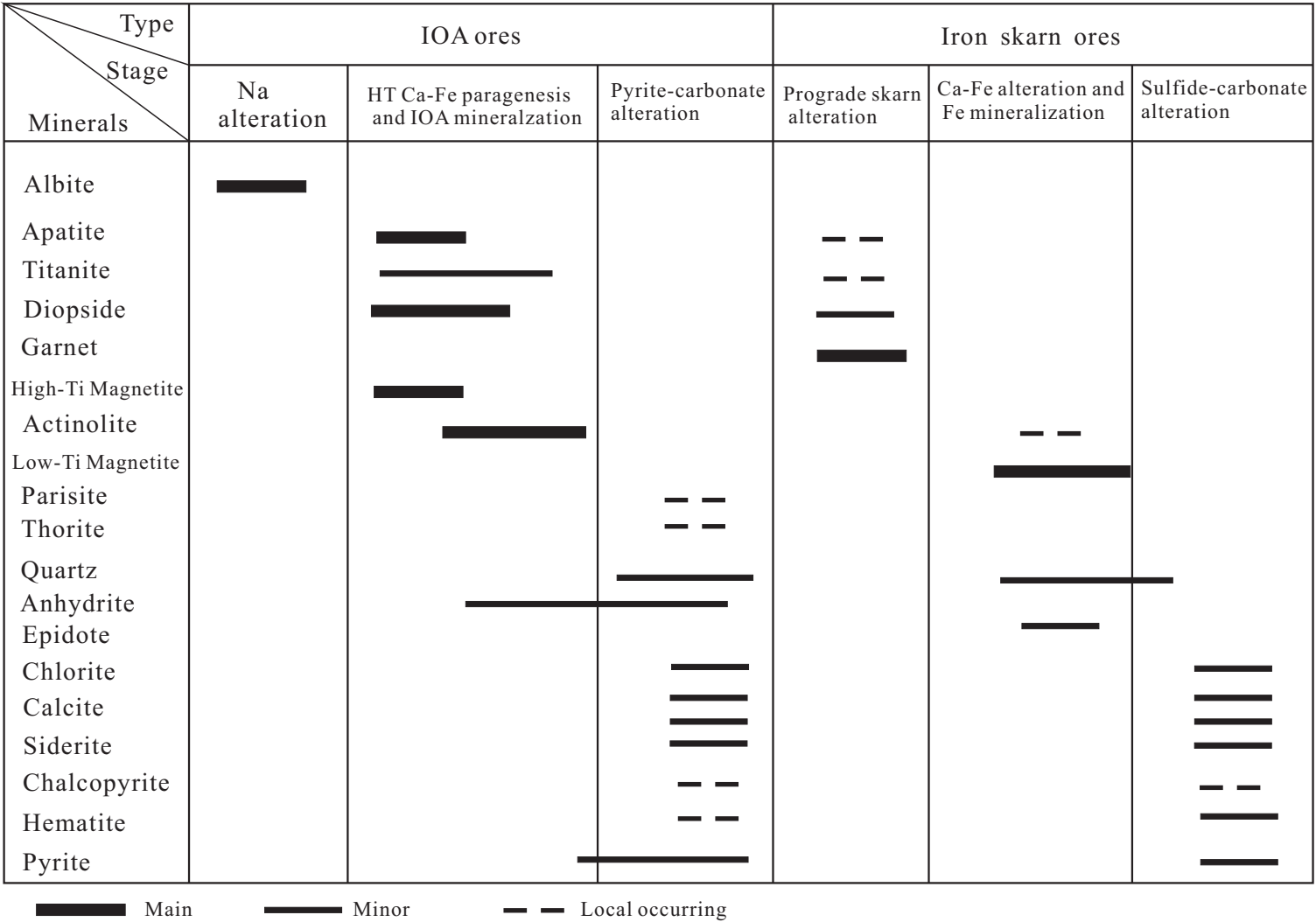
Type
Stage
Minerals
IOA ores
Iron skarn ores
Na alteration
HT Ca-Fe paragenesis and IOA mineralzation
Pyrite-carbonate alteration
Prograde skarn alteration
Ca-Fe alteration and Fe mineralization
Sulfide-carbonate alteration
Albite
Apatite
Titanite
Diopside
Garnet
High-Ti Magnetite
Actinolite
Low-Ti Magnetite
Parisite
Thorite
Quartz
Anhydrite
Epidote
Chlorite
Calcite
Siderite
Chalcopyrite
Hematite
Pyrite
Main
Minor
Local occurring

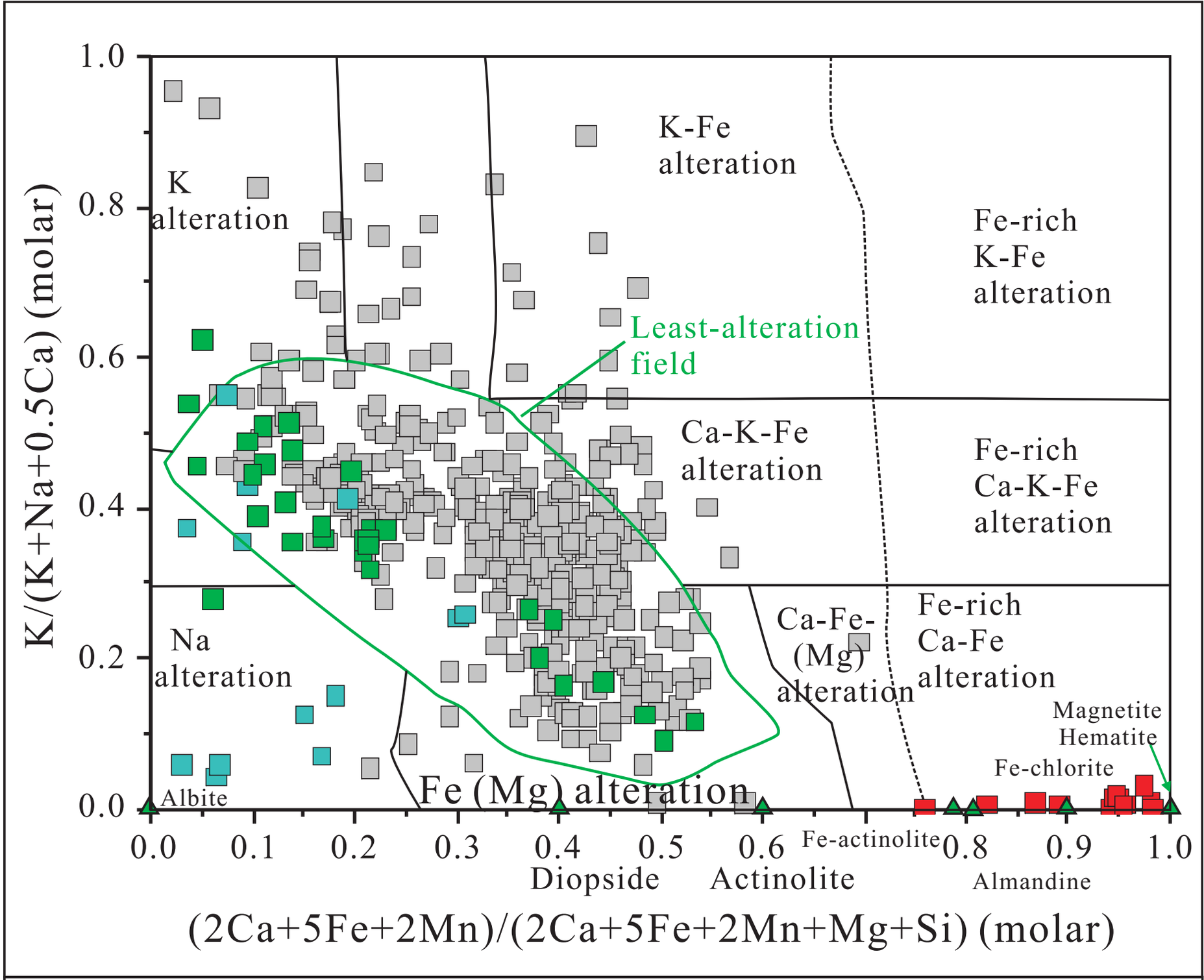

Iron-oxide apatite and iron skarn deposits related igneous rocks in Luzong and Ningwu districts

Volcanic rocks in Daye district

Granitiod host rock in iron skarn deposits

IOA and iron skarn ores in Wangbaoshan deposit

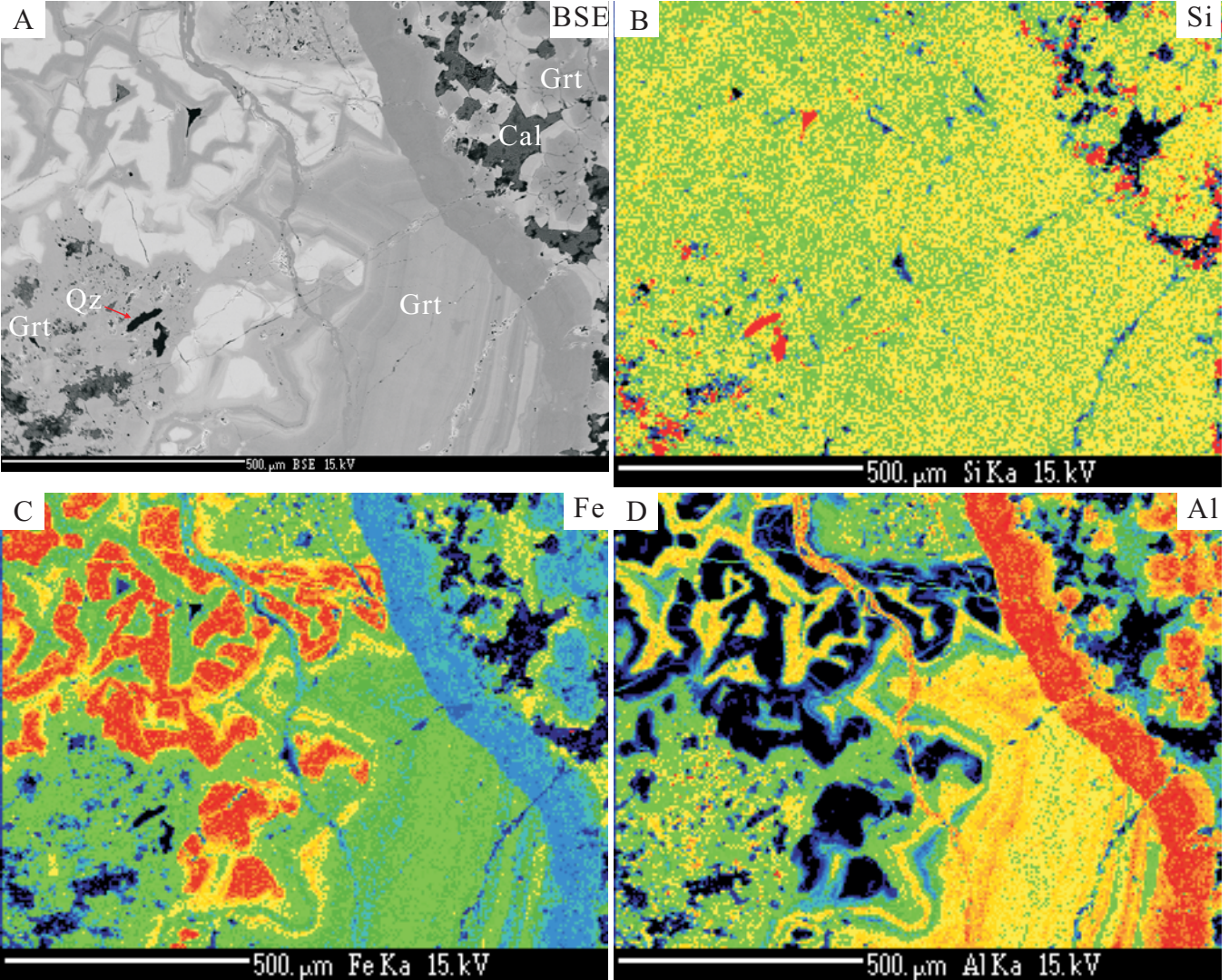
A
BSE
Grt
Cal
Qz
Grt
Grt
500.μm BSE 15.kV
B
Si
500.μm SiKa 15.kV
High
Low
C
Fe
500.μm FeKa 15.kV
D
Al
500.μm AlKa 15.kV

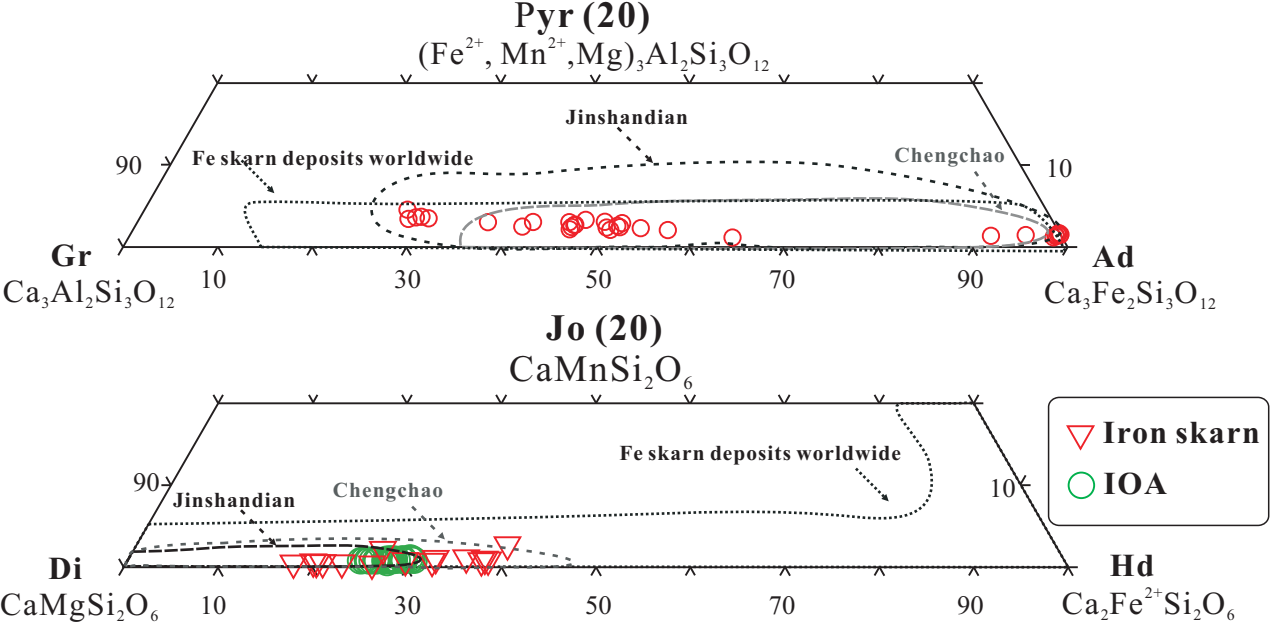
Pyr (20)
(Fe2+, Mn2+,Mg)3Al2Si3O12
Jinshandian
Fe skarn deposits worldwide
Chengchao
90
10
Gr
Ca3Al2Si3O12
10
30
50
70
90
Ad
Ca3Fe2Si3O12
Jo (20)
CaMnSi2O6
Fe skarn deposits worldwide
90
Jinshandian
Chengchao
10
Iron skarn
IOA
Di
CaMgSi2O6
10
30
50
70
90
Hd
Ca2Fe2+Si2O6